Electronic Structure of Naturally Occurring Aromatic Carbon

Andrew E. Pomerantz,*,†◉ Neil W. Bostrom,†,⊥ Robert L. Kleinberg,† Ethan Crace,‡,§
Tsu-Chien Weng,§,‖ Dimosthenis Sokaras,*,§ and Dennis Nordlund§

†Schlumberger-Doll Research, Cambridge, Massachusetts 02139, United States
‡Department of Chemistry, Stanford University, Stanford, California 94305, United States
§SLAC National Accelerator Laboratory, Menlo Park, California 94025, United States
‖Center for High Pressure Science & Technology Advanced Research, Shanghai 201203, China

HPSTAR
730-2019

ABSTRACT: Aromatic carbon in fused-ring systems can be classified into two forms of electronic structure: aromatic sextets, which have large highest occupied molecular orbital (HOMO)−lowest unoccupied molecular orbital (LUMO) gaps and resemble benzene; and isolated double bonds, which have small HOMO−LUMO gaps and resemble olefins. The relative abundance of aromatic sextets versus isolated double bonds in mixtures can be probed by carbon X-ray Raman spectroscopy. Here, we report the carbon X-ray Raman spectra of a wide variety of forms of naturally occurring aromatic carbon: kerogen (insoluble organic carbon in sedimentary rocks, which is the most abundant form of naturally occurring organic carbon in the Earth's crust) over a range of types and thermal maturities, fresh materials of a variety of forms, and coal and petroleum asphaltenes (toluene soluble and heptane insoluble materials, which represent organic carbon resulting from extensive thermal processing). It is observed that all these materials are dominated by aromatic sextets over isolated double bonds. On the basis of the diversity of materials analyzed, it is concluded that naturally occurring organic carbon is generally dominated by aromatic sextets over isolated double bonds. This conclusion is rationalized in terms of statistical and thermodynamic effects.

■ INTRODUCTION

Organic carbon undergoes many transformations during the carbon cycle, from atmospheric gases, to terrestrial and aquatic living organisms, to sedimentary forms such as kerogen and petroleum. Those transformations yield major changes in the molecular structure of organic carbon, from simple gases in the atmosphere to complex mixtures at the surface or buried in the subsurface. Even within a given set, the bulk molecular structure of organic matter varies greatly. For example, the composition of kerogen[1]—which is defined as insoluble organic matter in sedimentary rocks and is the most abundant form of naturally occurring organic carbon—evolves dramatically during the process of thermal maturation, with low-maturity kerogen being rich in heteroatoms and dominated by aliphatic carbon while high-maturity kerogen is lean in heteroatoms and dominated by aromatic carbon.[2−9] Similar evolutions have been observed in the composition of source rock bitumen,[10,11] petroleum,[12] and even the asphaltene fraction of petroleum.[13,14]

Despite extensive study, one aspect of the composition of organic carbon that has remained obscure is the electronic structure of aromatic moieties. The overall aromaticity of organic matter has been analyzed by tools such as infrared (IR) spectroscopy[8,15,16] and nuclear magnetic resonance (NMR) spectroscopy,[2,11,17−19] and the size and substitutions of fused aromatic ring systems have been further analyzed by NMR spectroscopy and optical spectroscopy.[5,14,20] However, these tools are not sensitive to the geometry of fused-ring systems or to certain aspects of the electronic structure of fused-ring systems. Indeed, an assumption about the geometry of fused-ring systems is required in the interpretation of NMR spectra to assign average molecular parameters such as the cluster size.[17,19]

The electronic structure of fused aromatic ring systems has been described by Clar,[21] expanding on the description of single aromatic rings from Hückel.[22−24] According to the heuristic described in the Clar model, π bonds in polycyclic aromatic hydrocarbons (PAHs) can consist of aromatic sextets and isolated double bonds.[21,25] Aromatic sextets are similar in structure and reactivity to benzene, and their π electrons are delocalized over the entire carbon hexagon. Aromatic sextets are the most aromatic centers in PAHs, and they indicate regions of local aromaticity in large molecules.[26,27] Aromatic sextets have large highest occupied molecular orbital (HOMO)−lowest unoccupied molecular orbital (LUMO) gaps because of electron delocalization, which makes these structures relatively stable.[28] Isolated double bonds, although they are also part of PAHs and consist of carbon that is entirely sp²-hybridized, are similar in structure and reactivity to olefinic double bonds in unconjugated molecules.[21,27,29] The π electrons in isolated double bonds are not delocalized over the entire carbon hexagon, so isolated double bonds have relatively small HOMO−LUMO gaps and are relatively unstable. Algorithms such as the Y-rule have been developed to identify regions composed of aromatic sextets and regions composed of isolated double bonds in PAHs, with the most probable electronic structure of a PAH being the one with maximum abundance of aromatic sextets and minimum abundance of isolated double bonds.[27,29−31]

One experimental technique that can probe the distribution of isolated double bonds and aromatic sextets in PAHs is carbon X-ray Raman spectroscopy.[32−35] Similar to a more conventional X-ray absorption spectroscopy, X-ray Raman spectroscopy measures electronic transitions from core orbitals to unoccupied orbitals with elemental specificity. However, in X-ray Raman spectroscopy, the transitions are studied via the Raman effect instead of direct absorption, similar to the study of vibrational transitions by Raman spectroscopy in the visible or near IR regions. Observing the carbon core electron spectra via X-ray Raman scattering instead of direct absorption allows the samples to be probed with hard X-rays (around 6700 eV) instead of soft X-rays (around 285 eV). The higher photon energy results in increased X-ray penetration depth (on the order of hundreds of microns to a millimeter), so carbon X-ray Raman spectroscopy is sensitive to bulk chemistry while carbon X-ray absorption spectroscopy interrogates surface chemistry (on the order of nanometers to microns). For materials that are prone to oxidation during sample preparation, such as naturally occurring organic carbon, bulk analysis may provide a more representative description of composition than can be obtained by surface measurement.

Starting in the early 2000s, some PAH model compounds and petroleum asphaltenes (PA) samples have been analyzed using carbon X-ray Raman spectroscopy.[19,36−38] Model compound studies indicated that linewidth of the X-ray Raman 1s−π* transition is sensitive to the electronic structure, with structures rich in aromatic sextets (such as coronene) giving rise to narrow lines and structures rich in isolated double bonds (such as tetracene) giving rise to broad lines. The asphaltene samples were found to yield spectra with narrow lines, suggesting that asphaltenes are dominated by aromatic sextets.

Recently, the spectra of the model PAH system were reanalyzed with a higher resolution X-ray Raman spectrometer.[35] With improved resolution, the previously observed broad line could be resolved as two separate peaks. Consistent with the previous results, the high-resolution spectra indicated that PAHs abundant in aromatic sextets give rise to singlet or narrowly separated doublets while PAHs abundant in isolated double bonds give rise to widely separated doublets. Additionally, the high-resolution results inspired an explanation of how the electronic structure, particularly the energetics of the LUMOs, controls the appearance of the X-ray Raman spectrum (see methods section for details).

Here, we present high-resolution X-ray Raman spectra of several forms of naturally occurring organic matter. Materials analyzed include fresh samples of living organisms, kerogen samples of varying type and thermal maturity, and asphaltenes. The spectra are analyzed with the high-resolution interpretation to assess the dominant electronic structures of fused-ring systems in various forms of terrestrial, aquatic, and sedimentary naturally occurring organic matter.

■ EXPERIMENTAL SECTION

X-ray Raman Spectroscopy. The X-ray Raman measurements and interpretations have been described previously and will be summarized briefly here.[35] Measurements were performed using the high-resolution X-ray Raman spectrometer operated at beamline 6−2 at the Stanford Synchrotron Radiation Laboratory.[34] The instrument consists of 40 crystal Si(440) analyzers arranged on overlapping Rowland circles of 1000 mm and at a fixed Bragg angle of 88°, resulting in a fixed detection energy at 6462 eV and an overall energy resolution of 0.29 eV. Spectra are recorded using an inverse scanning

approach, wherein the detection energy is held constant at 6462.2 eV while the incident energy is scanned through a Si(311) double-crystal monochromator over the range of 6732.2−6767.2 eV, resulting in an energy transfer range of 270−305 eV. The average momentum transfer is $q \approx 1.23$ a.u., which ensures that dipole transitions dominate the spectra and therefore the X-ray Raman spectra are formally equivalent to conventional soft X-ray absorption spectra.[39]

The interpretation of the X-ray Raman spectra has also been described previously and is summarized in Figure 1.[35] The figure
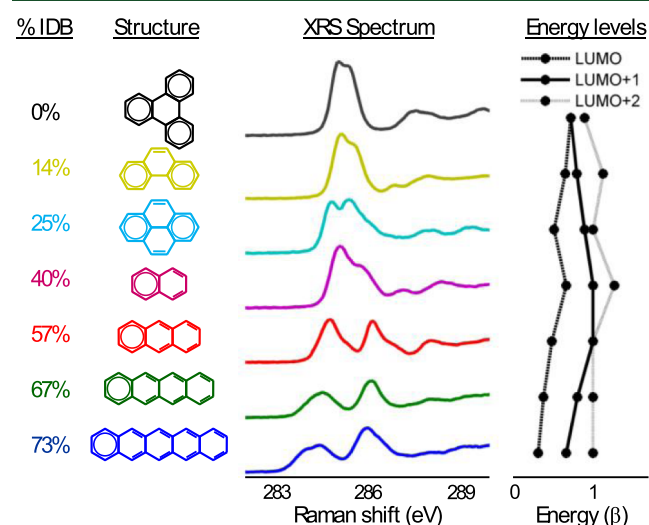
Figure 1. Schematic showing how X-ray Raman spectroscopy distinguishes between PAHs rich in aromatic sextets and PAHs rich in isolated double bonds.[35] Compounds are arranged from lowest to highest fraction of carbon contained in isolated double bonds (% IDB, defined as the number of carbon atoms in isolated double bonds divided by the number of carbon atoms in the molecule). Compounds lean in isolated double bonds (rich in aromatic sextets) yield spectra that are essentially singlets because the LUMO, LUMO + 1, and LUMO + 2 are nearly degenerate. Compounds rich in isolated double bonds (lean in aromatic sextets) yield spectra that are clearly resolved doublets because the LUMO, LUMO + 1, and LUMO + 2 are widely separated in energy. The far-right column displays the energies of the LUMO, LUMO + 1, and LUMO + 2, relative to the energy of the uncombined p orbitals, expressed in units of the Hückel resonance integral β.

shows the spectra of a series of PAH model compounds, arranged from compounds most abundant in aromatic sextets (top) to compounds most abundant in isolated double bonds (bottom). Structures depict the most probable configuration, according to the Clar model, with aromatic sextets drawn as inscribed circles such as in benzene and isolated double bonds drawn as unconjugated double bonds such as in olefins. Resonant structures with equal ratios of aromatic sextets to isolated double bonds are equally probable but are not drawn. Carbon X-ray Raman spectroscopy in this energy range probes transitions from carbon 1s orbitals to the LUMO and the next few higher-lying orbitals (LUMO + 1, LUMO + 2). Aromatic sextet carbon versus isolated double-bond carbon have large differences in LUMO energetics, with PAHs rich is aromatic sextets, having relatively high-lying LUMOs because of the large HOMO−LUMO gaps, while PAHs rich in isolated double bonds have relatively low-lying LUMOs. However, aromatic sextet carbon versus isolated double bond carbon have negligible differences in the energetics of the LUMO + 1 and LUMO + 2. Hence, for PAHs rich in aromatic sextets, the LUMO, LUMO + 1, and LUMO + 2 are nearly degenerate, and the measured X-ray Raman spectra—with represent the summed signals from transitions to all these states—are essentially singlets. For PAHs rich in isolated double bonds, these unoccupied energy levels are relatively widely spaced, and the measured X-ray
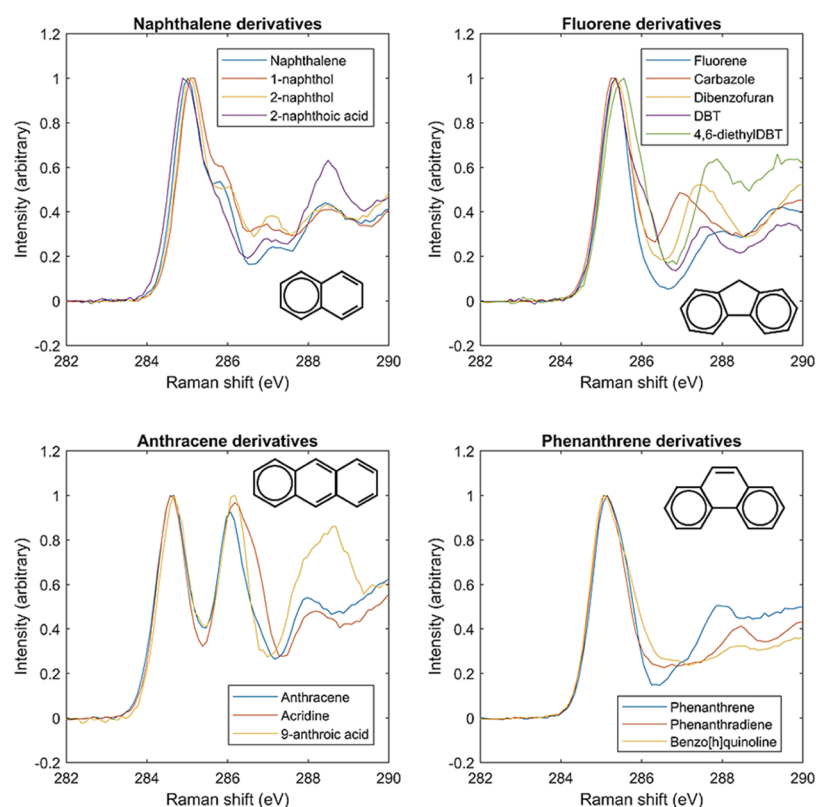
Figure 2. X-ray Raman spectra of four PAH model compounds along with oxygen-, sulfur-, and nitrogen-substituted analogs. DBT stands for dibenzothiophene. Heteroatoms substitutions are found to have minimal impact on the X-ray Raman spectra.

Raman spectra are doublets. In this way, carbon X-ray Raman spectroscopy probes the electronic structure of fused aromatic rings systems, distinguishing between systems rich in aromatic sextets and systems rich in isolated double bonds.

Unlike PAH model compounds that are pure hydrocarbons, naturally occurring organic compounds contain heteroatom substitutions, most often oxygen, sulfur, and nitrogen. To understand how those heteroatoms affect the X-Raman spectra, spectra were recorded for model PAHs as well as for substituted analogs. Figure 2 shows those results for four such systems. The heteroatoms are found to have minimal effect of the carbon X-ray Raman spectra, with the spectra of the heteroatom substituted analogs nearly overlaying the spectra of unsubstituted PAHs. As a result, the X-ray Raman interpretation described in Figure 1 for pure PAHs can be applied to heteroatom-containing PAHs (i.e., naturally occurring organic compounds) without modification.

Samples. Many of the samples analyzed here are kerogens (insoluble organic matter in sedimentary rocks).[1] In order to improve the signal-to-noise ratio, the kerogen samples (type I and II, described below) were concentrated by removing the majority of the mineral matter in the sedimentary rock by acid demineralization with hydrochloric and hydrofluoric acids.[40] No attempts were made to remove pyrite[41] or to preserve microstructure[42] because neither residual pyrite nor alterations to the microstructure influence these measurements of the electronic structure. This procedure resulted in concentrated kerogen isolates, with minimal impurities, that were presented to the X-ray beam.

Kerogens are categorized into different types, representing the initial hydrogen/carbon ratio and indicative of the dominant source material.[1,12] Type I kerogen is typically deposited in lacustrine environments and is prone to oil generation. Type II kerogen is typically deposited in marine environments and is prone to oil and gas generation; most economic oil and gas formations are sourced from type II kerogen. Type III kerogen is typically deposited in terrestrial environments and is prone to gas generation; most coal formations contain type III kerogen. Kerogen is also characterized by its thermal

maturity.[1,12] Maturation represents the extent to which the composition of kerogen has been altered from its initial structure due thermal degradation (pyrolysis). Maturation is often assessed by measuring the reflectance of the vitrinite maceral (VRo).[1,12,43,44] At low levels of maturity (below approximately 0.6% VRo), little degradation has occurred and kerogen is the dominant form of organic matter in the sedimentary rocks. At maturities in the range of approximately 0.6−0.8% VRo, some kerogen degradation has occurred, and the dominant form of organic matter is a soluble but viscous form referred to as source rock bitumen. At maturities in the range of approximately 0.8−1.35% VRo, significant kerogen degradation has occurred and oil is being generated. At high levels of maturity (above approximately 1.35% VRo), the generation of oil is essentially complete and additional pyrolysis generally leads to the generation of gas.

Samples analyzed here span a range of type and maturity. Type I samples were obtained from a fresh outcrop of the Eocene Green River Formation at the Mahogany Ledge location (Cathedral Creek) near the western edge of the Piceance Basin, Rio Blanco County, Colorado.[44] The immature outcrop was crushed, homogenized, and split into equivalent samples. The splits were artificially matured by semi-open pyrolysis, similar to that described previously.[8,11,13,14,45] X-ray Raman spectra were recorded for the low-maturity native state sample before pyrolysis (pyrolyzed for 0 h), samples with pre-oil window maturity (pyrolyzed for 4, 6 h), and samples from the oil window (pyrolyzed for 10, 24 h); see Figure 3. Type II samples were obtained from the Venezuelan La Luna formation, as described previously.[46] These samples range in maturity from prior to oil generation to overmature (0.4−2.7% VRo). Type III samples were obtained from the Department of Energy Coal Sample Bank & Database (DECS).[47] Specific samples scanned include DECS-5 (VRo = 0.59%), DECS-10 (VRo = 0.42%), DECS-11 (VRo = 0.35%), DECS-15 (VRo = 0.80%), DECS-19 (VRo = 1.71%), DECS-21 (VRo = 5.19%), and DECS-30 (VRo = 1.16%). An additional set of type III samples were obtained as coals from the Illinois Basin, as described previously.[48,49]
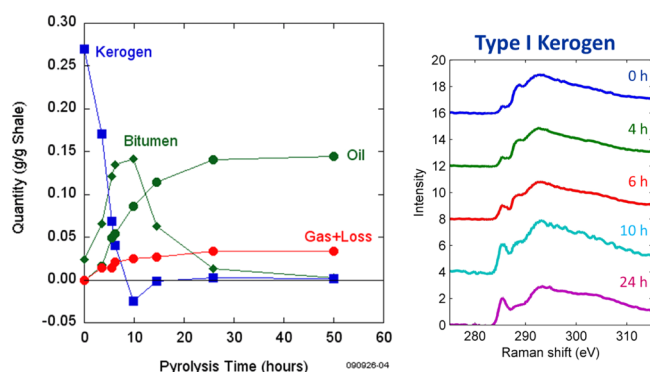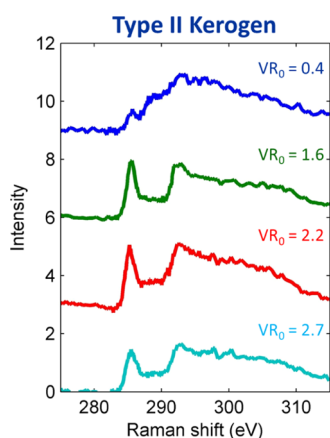
Figure 3. X-ray Raman spectra of type I kerogens. The left panel shows the abundance of different organic phases, relating the pyrolysis time to the thermal maturity. The right panel shows the spectra of five samples with different thermal maturities.

In addition to kerogens, samples scanned here also included four fresh materials. These materials are representative of precursors to type I kerogen (algae) and type III kerogen (fern, rhododendron, and peat). All fresh materials were sampled immediately prior to X-ray Raman measurement and were analyzed without any preparation. Finally, samples scanned also included asphaltenes, which are the fraction of a mixture that dissolves in aromatic solvent (such as toluene) but not in aliphatic solvent (such as heptane). Asphaltenes were extracted from petroleum, so they represent the material generated during the thermal maturation process. The asphaltene extraction process involved diluting the crude oil in 40-fold excess of n-heptane, stirring for 24 h, recovering the precipitated asphaltenes by filtration through a nylon membrane with 0.65 μm pores, and washing the precipitated asphaltenes with additional n-heptane briefly on the nylon membrane and then for two days in a Soxhlet extractor.[50] Asphaltenes were also extracted from coal, as described previously.[19,50−52]

■ **RESULTS**

X-ray Raman spectra of the naturally occurring organic materials are presented in Figures 3−7. The spectra are


**Figure 4.** X-ray Raman spectra of type II kerogens. Samples are labeled by their thermal maturities.

presented over a wider range than shown for the model compounds in Figures 1 and 2. This range contains a 1s−π* transition centered around 285 eV Raman shift and representative of aromatic carbon, a 1s−σ* transition centered around 288 eV Raman shift and representative of aliphatic carbon, and a featureless postedge region above approximately
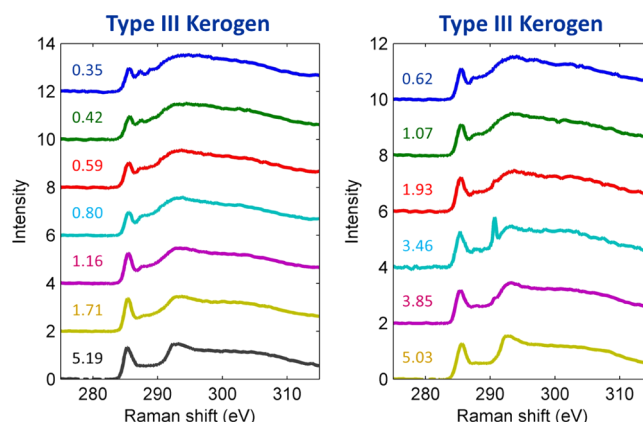
Figure 5. X-ray Raman spectra of type III kerogens (coals). The left panel shows spectra representing samples from the Department of Energy Coal Sample Bank & Database.[47] The right panel shows spectra representing coals from the Illinois Basin.[48,49] Samples are labeled by their thermal maturities.
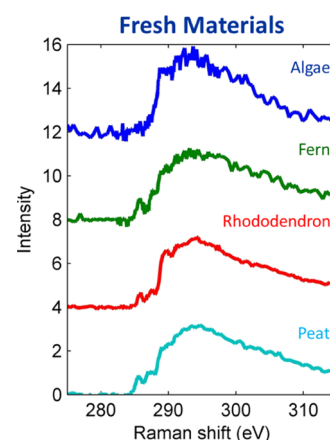
Figure 6. X-ray Raman spectra of fresh materials.
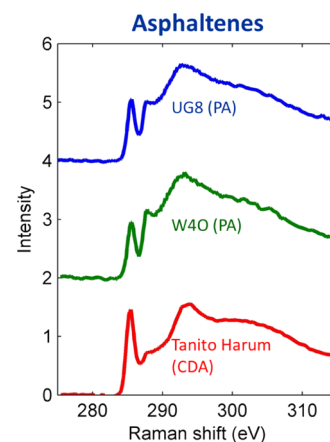
Figure 7. X-ray Raman spectra of PAs and CDAs.

290 eV Raman shift.[53] The 1s−π* transition can appear as a singlet (indicative of the dominance of aromatic sextets) or as a doublet (indicative of the dominance of isolated double bonds) as discussed above.

Figure 3 presents the X-ray Raman spectra of type I kerogens spanning a range of thermal maturities. The most pronounced difference between the spectra is that the low-

maturity samples present a strong 1s−σ* peak but only a weak 1s−π* peak, while the intensity of the peaks is reversed in the spectra of the high-maturity samples. This trend is consistent with enrichment in aromatic carbon and a loss in aliphatic carbon during kerogen maturation.[2,45] Meanwhile, the line-shape of the 1s−π* transition remains constant as a narrow singlet at all thermal maturities investigated here. This result indicates that aromatic carbon in type I kerogen is dominated by aromatic sextets, rather than isolated double bonds, across this range of thermal maturity.

Similar results are observed in all the other spectra recorded here. The 1s−π* lineshape remains constant as a narrow singlet for all the type II kerogens (Figure 4) and for both sets of the type III kerogens (Figure 5), over all thermal maturities analyzed. The trend of 1s−π* intensity increasing and 1s−σ* intensity decreasing at higher thermal maturities is observed in many of these samples. The spectra of the fresh materials (Figure 6) are somewhat noisy with weak 1s−π* peaks, but the 1s−π* lineshape remains constant as a narrow singlet for all samples studied here. This result is consistent with these materials being rich in structures like lignin, in which the concentration of aromatic carbon is relatively low and the composition of the aromatic carbon is dominated by aromatic sextets. The spectra of the petroleum and coal-derived asphaltenes (CDA) (Figure 7) show more intense 1s−σ* peaks for PAs (50% aliphatic carbon) than for the CDAs (15% aliphatic carbon), as expected. Again, the 1s−π* lineshape remains constant as a narrow singlet for all asphaltenes analyzed here. The observed dominance of aromatic sextets over isolated double bonds in petroleum and CDAs is consistent with earlier X-ray Raman results[36−38] as well as recent atomic force microscopy[51,52] results.

■ DISCUSSION

It is observed, in all the samples studied here, that aromatic carbon is dominated by aromatic sextets rather than isolated double bonds. Given the diversity of samples studied here—kerogens (which are the dominant form of naturally occurring organic carbon in the Earth's crust)[1] over a wide range of type and maturity, fresh materials, and products of petroleum generation (asphaltenes)—it can be concluded that naturally occurring organic carbon is generally dominated by aromatic sextets rather than isolated double bonds.

There are two main factors that contribute to the dominance of aromatic sextets in naturally occurring organic carbon. The first factor is statistics. Isolated double bonds are dominant only in PAHs that are linearly concatenated, such as anthracene, tetracene, or pentacene components. For structures with a large number of fused rings, there are more potential configurations for fused-ring structures that are not perfectly linearly concatenated than that are perfectly linearly concatenated. From a statistical perspective, when nature generates structures with many fused aromatic rings, there is a greater likelihood for the structures to contain abundant aromatic sextets than for the structures to contain abundant isolated double bonds. This argument holds for the PAs and coal-derived asphaltenes (25−30 aromatic carbons per fused-ring system),[19] as well as for mature kerogens (approximately 20 aromatic carbons per fused-ring system).[2] Similarly, benzene is a fully aromatic sextet, and the smallest PAH that displays a pronounced doublet structure in the X-ray Raman spectra is anthracene (14 carbons). From a statistical perspective, when nature generates structures with few fused

aromatic rings, there is no opportunity for the structures to contain abundant isolated double bonds. This argument holds for immature kerogens (approximately 10 aromatic carbons per fused-ring system)[2] and for fresh materials, which are composed largely of lignin structures that contain single-ring systems. Thus, the statistical likelihood for naturally occurring fused-ring systems to be dominated by isolated double bonds is constrained on both ends of the size distribution.

The second factor is thermodynamics. Because isolated double bonds are less stable than aromatic sextets, structures with large numbers of isolated double bonds are much less stable than structures with large numbers of aromatic sextets. For example, coronene (24 carbons, dominated by aromatic sextets) is stable for geologic time, whereas heptacene (30 carbons, dominated by isolated double bonds) has a half-life of several weeks at room temperature.[54] Materials that survive for geologic time cannot be dominated by unstable moieties. Thus, all samples studied here save for the fresh material are expected from thermodynamics to be dominated by aromatic sextets rather than isolated double bonds.

Combining these two factors, the only opportunity for nature to generate fused-ring systems dominated by isolated double bonds lies in young materials that are not constrained to consist of highly stable structures capable of surviving geologic time, wherein either the isolated double-bond structure serves a specific biological function or the aromatic systems consist of a moderate number of fused rings, where abundant isolated double-bond structures are statistically likely. It appears that nature does not create such structures in great abundance.

■ CONCLUSIONS

Fused aromatic ring systems contain aromatic sextets (similar to benzene) and isolated double bonds (similar to olefins). Carbon X-ray Raman spectroscopy is an experimental technique capable of measuring the relative abundance of aromatic sextets versus isolated double bonds in mixtures. By measuring the X-ray Raman spectra of a wide variety of forms of naturally occurring organic carbon—kerogens (which are the dominant form of naturally occurring organic carbon in the Earth's crust) over a wide range of type and maturity, fresh material, and products of petroleum generation (asphaltenes)—it is concluded that naturally occurring organic carbon is generally dominated by aromatic sextets. The widespread occurrence of aromatic sextets in nature is driven partially by statistics, as structures dominated by isolated double bonds are statistically unlikely for fused-ring systems with small (<14) or large (>20) numbers of carbons. The widespread occurrence of aromatic sextets in nature is also driven partially by thermodynamics, as structures with large numbers of isolated double bonds lack the stability to survive for geologic time.

■ AUTHOR INFORMATION

Corresponding Authors
*E-mail: apomerantz@slb.com (A.E.P.).
*E-mail: dsokaras@slac.stanford.edu (D.S.).

ORCID ⊙
Andrew E. Pomerantz: 0000-0003-2639-2682

Present Address
⊥Varex Imaging, Salt Lake City, UT 84104 USA.

Notes
The authors declare no competing financial interest.

■ REFERENCES

(1) Durand, B. Sedimentary organic matter and kerogen. Definition and quantitative importance of kerogen. In *Kerogen: Insoluble Organic Matter from Sedimentary Rocks*; Durand, B., Ed.; Editions Technip: Paris, 1980.

(2) Kelemen, S. R.; Afeworki, M.; Gorbaty, M. L.; Sansone, M.; Kwiatek, P. J.; Walters, C. C.; Freund, H.; Siskin, M.; Bence, A. E.; Curry, D. J.; Solum, M.; Pugmire, R. J.; Vandenbroucke, M.; Leblond, M.; Behar, F. Direct Characterization of Kerogen by X-ray and Solid-State ^{13}C Nuclear Magnetic Resonance Methods. *Energy Fuels* 2007, *21*, 1548−1561.

(3) Kelemen, S. R.; Fang, H. L. Maturity Trends in Raman Spectra from Kerogen and Coal. *Energy Fuels* 2001, *15*, 653−658.

(4) Pomerantz, A. E. Toward Molecule-Specific Geochemistry of Heavy Ends: Application to the Upstream Oil Industry. *Ind. Eng. Chem. Res.* 2016, *55*, 4403−4414.

(5) Ferralis, N.; Liu, Y.; Bake, K. D.; Pomerantz, A. E.; Grossman, J. C. Direct correlation between aromatization of carbon-rich organic matter and its visible electronic absorption edge. *Carbon* 2015, *88*, 139−147.

(6) Thomas, J. J.; Valenza, J. J.; Craddock, P. R.; Bake, K. D.; Pomerantz, A. E. The neutron scattering length density of kerogen and coal as determined by CH_3OH/CD_3OH exchange. *Fuel* 2014, *117*, 801−808.

(7) Cheshire, S.; Craddock, P. R.; Xu, G.; Sauerer, B.; Pomerantz, A. E.; McCormick, D.; Abdallah, W. Assessing thermal maturity beyond the reaches of vitrinite reflectance and Rock-Eval pyrolysis: A case study from the Silurian Qusaiba formation. *Int. J. Coal Geol.* 2017, *180*, 29−45.

(8) Craddock, P. R.; Le Doan, T. V.; Bake, K.; Polyakov, M.; Charsky, A. M.; Pomerantz, A. E. Evolution of Kerogen and Bitumen during Thermal Maturation via Semi-Open Pyrolysis Investigated by Infrared Spectroscopy. *Energy Fuels* 2015, *29*, 2197−2210.

(9) Craddock, P. R.; Bake, K. D.; Pomerantz, A. E. Chemical, Molecular, and Microstructural Evolution of Kerogen during Thermal Maturation: Case Study from the Woodford Shale of Oklahoma. *Energy Fuels* 2018, *32*, 4859−4872.

(10) Bolin, T. B.; Birdwell, J. E.; Lewan, M. D.; Hill, R. J.; Grayson, M. B.; Mitra-Kirtley, S.; Bake, K. D.; Craddock, P. R.; Abdallah, W.; Pomerantz, A. E. Sulfur Species in Source Rock Bitumen before and after Hydrous Pyrolysis Determined by X-ray Absorption Near-Edge Structure. *Energy Fuels* 2016, *30*, 6264−6270.

(11) Feng, Y.; Le Doan, T. V.; Pomerantz, A. E. The Chemical Composition of Bitumen in Pyrolyzed Green River Oil Shale: Characterization by ^{13}C NMR Spectroscopy. *Energy Fuels* 2013, *27*, 7314−7323.

(12) Peters, K. E.; Walters, C. C.; Moldowan, J. M. *The Biomarker Guide*. 2 ed.; Cambridge University Press: Cambridge, 2005; Vol. 1.

(13) Pomerantz, A. E.; Le Doan, T. V.; Craddock, P. R.; Bake, K. D.; Kleinberg, R. L.; Burnham, A. K.; Wu, Q.; Zare, R. N.; Brodnik, G.; Lo, W. C. H.; Grayson, M.; Mitra-Kirtley, S.; Bolin, T. B.; Wu, T. Impact of Laboratory-Induced Thermal Maturity on Asphaltene Molecular Structure. *Energy Fuels* 2016, *30*, 7025−7036.

(14) Bake, K. D.; Pomerantz, A. E. Optical Analysis of Pyrolysis Products of Green River Oil Shale. *Energy Fuels* 2017, *31*, 13345−13352.

(15) Craddock, P. R.; Prange, M. D.; Pomerantz, A. E. Kerogen thermal maturity and content of organic-rich mudrocks determined using stochastic linear regression models applied to diffuse reflectance

IR Fourier transform spectroscopy (DRIFTS). *Org. Geochem.* 2017, *110*, 122−133.

(16) Washburn, K. E.; Birdwell, J. E. Multivariate analysis of ATR-FTIR spectra for assessment of oil shale organic geochemical properties. *Org. Geochem.* 2013, *63*, 1−7.

(17) Solum, M. S.; Pugmire, R. J.; Grant, D. M. ^{13}C Solid-State NMR of Argonne Premium Coals. *Energy Fuels* 1989, *3*, 187−193.

(18) Solum, M. S.; Mayne, C. L.; Orendt, A. M.; Pugmire, R. J.; Adams, J.; Fletcher, T. H. Characterization of Macromolecular Structure Elements from a Green River Oil Shale, I. Extracts. *Energy Fuels* 2013, *28*, 453−465.

(19) Andrews, A. B.; Edwards, J. C.; Pomerantz, A. E.; Mullins, O. C.; Nordlund, D.; Noringa, K. Comparison of Coal-Derived and Petroleum Asphaltenes by ^{13}C Nuclear Magnetic Resonance, DEPT, and XRS. *Energy Fuels* 2011, *25*, 3068−3076.

(20) Mullins, O. C.; Mitra-Kirtley, S.; Zhu, Y. The Electronic Absorption Edge of Petroleum. *Appl. Spectrosc.* 1992, *46*, 1405−1411.

(21) Clar, E. *The Aromatic Sextet*; John Wiley & Sons: London, 1972; p 128.

(22) Hückel, E. Quantentheoretische Beitrage zum Benzolproblem. *Z. Phys.* 1931, *70*, 204−286.

(23) Hückel, E. Quantentheoretische Beitrage zum Benzolproblem II. *Eur. Phys. J. A* 1931, *72*, 310−337.

(24) Hückel, E.; Hückel, E. Quantentheoretische Beitrage zum Problem der ̈aromatischen und ungesattigten Verbindungen. III. *Z. Phys.* 1932, *76*, 628−648.

(25) Sola, M. Forty years of Clar's aromatic pi-sextet rule. *Front. Chem.* 2013, *1*, 22.

(26) Portella, G.; Poater, J.; Solà, M. Assessment of Clar's aromatic π-sextet rule by means of PDI, NICS and HOMA indicators of local aromaticity. *J. Phys. Org. Chem.* 2005, *18*, 785−791.

(27) Vijayalakshmi, K. P.; Suresh, C. H. Pictorial representation and validation of Clar's aromatic sextet theory using molecular electrostatic potentials. *New J. Chem.* 2010, *34*, 2132.

(28) Aihara, J.-i. Reduced HOMO-LUMO Gap as an Index of Kinetic Stability for Polycyclic Aromatic Hydrocarbons. *J. Phys. Chem. A* 1999, *103*, 7487−7495.

(29) Ruiz-Morales, Y. The Agreement between Clar Structures and Nucleus-Independent Chemical Shift Values in Pericondensed Benzenoid Polycyclic Aromatic Hydrocarbons: An Application of the Y-Rule. *J. Phys. Chem. A* 2004, *108*, 10873−10896.

(30) Oña-Ruales, J. O.; Ruiz-Morales, Y. Extended Y-rule method for the characterization of the aromatic sextets in cata-condensed polycyclic aromatic hydrocarbons. *J. Phys. Chem. A* 2014, *118*, 12262−12273.

(31) Randić, M. Aromaticity of Polycyclic Conjugated Hydrocarbons. *Chem. Rev.* 2003, *103*, 3449−3606.

(32) Bergmann, U.; Glatzel, P.; Cramer, S. P. Bulk-sensitive XAS characterization of light elements: from X-ray Raman scattering to X-ray Raman spectroscopy. *Microchem. J.* 2002, *71*, 221−230.

(33) Gordon, M. L.; Tulumello, D.; Cooper, G.; Hitchcock, A. P.; Glatzel, P.; Mullins, O. C.; Cramer, S. P.; Bergmann, U. Inner-Shell Excitation Spectroscopy of Fused-Ring Aromatic Molecules by Electron Energy Loss and X-ray Raman Techniques. *J. Phys. Chem. A* 2003, *107*, 8512−8520.

(34) Sokaras, D.; Nordlund, D.; Weng, T. C.; Mori, R. A.; Velikov, P.; Wenger, D.; Garachtchenko, A.; George, M.; Borzenets, V.; Johnson, B.; Qian, Q.; Rabedeau, T.; Bergmann, U. A high resolution and large solid angle x-ray Raman spectroscopy end-station at the Stanford Synchrotron Radiation Lightsource. *Rev. Sci. Instrum.* 2012, *83*, 043112.

(35) Pomerantz, A. E.; Crace, E.; Weng, T.-C.; Sokaras, D.; Nordlund, D. Carbon Core Electron Spectra of Polycyclic Aromatic Hydrocarbons. *J. Phys. Chem. A* 2018, *122*, 5730−5734.

(36) Bergmann, U.; Mullins, O. C.; Cramer, S. P. X-ray Raman Spectroscopy of Carbon in Asphaltene: Light Element Characterization with Bulk Sensitivity. *Anal. Chem.* 2000, *72*, 2609−2612.

(37) Bergmann, U.; Groenzin, H.; Mullins, O. C.; Glatzel, P.; Fetzer, J.; Cramer, S. P. Carbon K-edge X-ray Raman spectroscopy supports

simple, yet powerful description of aromatic hydrocarbons and asphaltenes. *Chem. Phys. Lett.* **2003**, *369*, 184−191.

(38) Bergmann, U.; Groenzin, H.; Mullins, O. C.; Glatzel, P.; Fetzer, J.; Cramer, S. P. X-Ray Raman Spectroscopy–A New Tool to Study Local Structure of Aromatic Hydrocarbons and Asphaltenes. *Pet. Sci. Technol.* **2004**, *22*, 863−875.

(39) Schülke, W. *Electron Dynamics by Inelastic X-Ray Scattering*; OUP Oxford: Oxford, 2007.

(40) Durand, B.; Nicaise, G. Procedures for kerogen isolation. In *Kerogen: Insoluble Organic Matter from Sedimentary Rocks*; Durand, B., Ed.; Editions Technip: Paris, 1980.

(41) Acholla, F. V.; Orr, W. L. Pyrite Removal from Kerogen without Altering Organic Matter: The Chromous Chloride Method. *Energy Fuels* **1993**, *7*, 406−410.

(42) Suleimenova, A.; Bake, K. D.; Ozkan, A.; Valenza, J. J.; Kleinberg, R. L.; Burnham, A. K.; Ferralis, N.; Pomerantz, A. E. Acid demineralization with critical point drying: A method for kerogen isolation that preserves microstructure. *Fuel* **2014**, *135*, 492−497.

(43) Dembicki, H. Three common source rock evaluation errors made by geologists during prospect or play appraisals. *AAPG Bull.* **2009**, *93*, 341−356.

(44) Peters, K. E.; Hackley, P. C.; Thomas, J. J.; Pomerantz, A. E. Suppression of vitrinite reflectance by bitumen generated from liptinite during hydrous pyrolysis of artificial source rock. *Org. Geochem.* **2018**, *125*, 220−228.

(45) Le Doan, T. V.; Bostrom, N. W.; Burnham, A. K.; Kleinberg, R. L.; Pomerantz, A. E.; Allix, P. Green River Oil Shale Pyrolysis: Semi-Open Conditions. *Energy Fuels* **2013**, *27*, 6447−6459.

(46) Simoneit, B. R. T.; Brenner, S.; Peters, K. E.; Kaplan, I. R. Thermal alteration of Cretaceous black shale by basaltic intrusions in the Eastern Atlantic. *Nature* **1978**, *273*, 501.

(47) http://www.energy.psu.edu/csb/doesb.html; accessed December 27, 2018.

(48) Mastalerz, M.; Drobniak, A.; Schimmelmann, A. Changes in optical properties, chemistry, and micropore and mesopore characteristics of bituminous coal at the contact with dikes in the Illinois Basin. *Int. J. Coal Geol.* **2009**, *77*, 310−319.

(49) Schimmelmann, A.; Mastalerz, M.; Gao, L.; Sauer, P. E.; Topalov, K. Dike intrusions into bituminous coal, Illinois Basin: H, C, N, O isotopic responses to rapid and brief heating. *Geochim. Cosmochim. Acta* **2009**, *73*, 6264−6281.

(50) Wang, W.; Taylor, C.; Hu, H.; Humphries, K. L.; Jaini, A.; Kitimet, M.; Scott, T.; Stewart, Z.; Ulep, K. J.; Houck, S.; Luxon, A.; Zhang, B.; Miller, B.; Parish, C. A.; Pomerantz, A. E.; Mullins, O. C.; Zare, R. N. Nanoaggregates of Diverse Asphaltenes by Mass Spectrometry and Molecular Dynamics. *Energy Fuels* **2017**, *31*, 9140−9151.

(51) Schuler, B.; Fatayer, S.; Meyer, G.; Rogel, E.; Moir, M.; Zhang, Y.; Harper, M. R.; Pomerantz, A. E.; Bake, K. D.; Witt, M.; Peña, D.; Kushnerick, J. D.; Mullins, O. C.; Ovalles, C.; van den Berg, F. G. A.; Gross, L. Heavy Oil Based Mixtures of Different Origins and Treatments Studied by Atomic Force Microscopy. *Energy Fuels* **2017**, *31*, 6856−6861.

(52) Schuler, B.; Meyer, G.; Peña, D.; Mullins, O. C.; Gross, L. Unraveling the Molecular Structures of Asphaltenes by Atomic Force Microscopy. *J. Am. Chem. Soc.* **2015**, *137*, 9870−9876.

(53) Stöhr, J. *NEXAFS Spectroscopy*; Springer: Berlin, 1992; p 403.

(54) Einholz, R.; Fang, T.; Berger, R.; Grüninger, P.; Früh, A.; Chassé, T.; Fink, R. F.; Bettinger, H. F. Heptacene: Characterization in Solution, in the Solid State, and in Films. *J. Am. Chem. Soc.* **2017**, *139*, 4435−4442.